Applied Catalysis B: Environmental 160–161 (2014) 415–422

Contents lists available at ScienceDirect

Applied Catalysis B: Environmental

journal homepage: www.elsevier.com/locate/apcatb

The role of cobalt and nickel in deoxygenation of vegetable oils

Haiping Zhang, Hongfei Lin, Ying Zheng*

Department of Chemical Engineering, University of New Brunswick, Head Hall, 15 Dineen Drive, Fredericton, NB, Canada, E3B 5A3

ARTICLE INFO

Article history:
Received 25 January 2014
Received in revised form 16 May 2014
Accepted 23 May 2014
Available online 2 June 2014

Keyword:
Hydrodeoxygenation (HDO)
Hydrodecarbonylation/decarboxylation (HDC)
Unsupported catalyst
NiMoS
CoMoS

ABSTRACT

Nickel (Ni)/cobalt (Co) promoted MoS_2 catalysts have been recently studied in deoxygenation of vegetable oils. Ni and Co play a key role in enhancing the catalytic activities and selectivity of MoS_2. To better understand their functions, nanosized unsupported NiMoS and CoMoS catalysts were studied in this work. Without the influence of catalyst supports, the inherent impact of nickel and cobalt on the main deoxygenation routes has been investigated. Ni-promoted catalyst exhibits higher selectivity for hydrodeoxygenation (HDO) reaction over hydrodecarbonylation/decarboxylation (HDC), while Co-promoted catalyst prefers HDC. Based on the analysis of upgraded products and catalysts, a new insight was proposed to interpret the impact of catalyst structure on deoxygenation pathways. NiMoS creates abundant sulfur vacancies that improve the hydrogenation ability; CoMoS catalyst shows saturated edge sites in hydrogen atmosphere, facilitating the hydrocracking (C—C hydrogenolysis). The enhancement of HDO reaction by Ni is primarily realized through the synergy effect of Mo and Ni on unsaturated sites of metal edge. By contrast, the HDC reaction is facilitated by Co-promoted MoS_2 through adsorption of C atoms on the S edge that is adjacent to Co.

1. Introduction

Nickel (Ni)/cobalt (Co)-promoted molybdenum (Mo)-based catalysts are commonly used in hydrodesulfurization of petroleum fractions. They have recently been applied to the processes in elimination of oxygen from plant oils (deoxygenation, hereafter) [1–7]. Two main reaction routes were identified in the deoxygenation process, namely hydrodecarbonylation/decarboxylation (HDC) and hydrodeoxygenation (HDO) [3,4]. HDC involves C—C bond breakage producing hydrocarbons with one carbon number less than their corresponding fatty acids, while the HDO reaction produces hydrocarbons of the same carbon number as the fatty acids in triglycerides. Since most triglycerides contain 18 carbons in chains, C_{18}/C_{17} ratio has then been used to identify primary deoxygenation reaction routes [4]. Many reports suggested that HDO dominates reaction pathways in the hydrotreating of triglycerides regardless the type of promoters [4–8]. Krar et al. supported the statement by producing the C_{18}/C_{17} ratios between 3 and 20 over Co-promoted catalyst [9]. Again with Co-promoted catalyst, Toba et al. confirmed that C_{18} was a dominant product by hydrotreating waste cooking oil [8]. Similar C_{18}/C_{17} ratios were observed when Ni-promoted catalysts were employed [6,8]. However, other research groups showed different observations. Bezergianni et al. showed that more C_{17} was produced and the C_{18}/C_{17} ratios were less than one when waste cooking oil was hydrodeoxygenated over Ni-MoS_2 [10]. Low C_{18}/C_{17} ratio (<1) was also obtained when hydrotreating refined rapeseed oil under 2.3 MPa hydrogen pressure over supported Co-MoS_2 [11]. The conflict observations raised different views of the roles of promoters in the deoxygenation reaction. However, very limited research has been carried out to understand the functions of different promoters.

Catalyst support can significantly affect deoxygenation reaction. Centeno et al. investigated the effects of different support materials and stated that acidity of support materials can enhance the formation of active sites for both decarboxylation and hydrogenation of carboxyl groups [12]. Other studies also observed that catalyst support, e.g. alumina, alone had catalytic activity due to its Lewis acid sites [13]. To understand the role of promoters, the effect of supporting material has to be eliminated. Unsupported Co and Ni promoted MoS_2 catalysts were synthesized using a hydrothermal method [14]. The present work aims to understand the promoting impact of Ni and Co on the deoxygenation performance of MoS_2 and the reaction pathways of oxygen removal.

2. Experimental

2.1. Catalyst synthesis and characterization

Unsupported catalysts CoMoS and NiMoS were synthesized by the reported hydrothermal method [14]. Precursors MoO_3,

* Corresponding author. Tel.: +1 506 447 3329.
E-mail address: yzheng@unb.ca (Y. Zheng).

http://dx.doi.org/10.1016/j.apcatb.2014.05.043
0926-3373/

$Na_2S{\cdot}9H_2O$, HCl, $Co(NO_3)_2{\cdot}6H_2O$ and $Ni(NO_3)_2{\cdot}6H_2O$ were purchased from STEM and Fisher Scientific and used as received. The mixture of precursors was first dissolved in deionized water and then introduced into an autoclave reactor. The hydrothermal reaction took place at 320 °C and lasted for 2 h under the stirring speed of 500 rpm. After reaction, the resultant black solid was separated and washed by deionized water and ethanol without nitrogen protection. The catalysts were then dried under nitrogen at 120 °C for 4 h. They have good chances to contact air during washing and storage. In order to eliminate any oxidization that may occur, the catalysts were sulfided at 280 °C for 2 h in the presence of dimethyl disulfide before evaluation.

The morphology of the synthesized catalyst was analyzed by a transmission electron microscopy (JEOL 2011 STEM, JEOL Ltd., Tokyo, Japan). The crystalline sizes of CoMoS and NiMoS were measured using image analysis software and the average sizes were calculated based on 100+ slabs of various particles. The amount of cobalt and nickel incorporated was estimated by energy-dispersive X-ray spectroscopy (EDX). The specific surface area of catalysts was measured on an Autosorb-1 (Quantachrome Instruments, Florida, US) using the Brunauer–Emmett–Teller (BET) method. The pore size distribution of the catalyst powders was determined from the obtained isotherms using the Barrett–Joyner–Halenda (BJH) method. The sulfur content in fresh and spent catalyst was tested on a CHNS-O 932 elemental analyzer (LECO Corporation, MI, US).

Temperature programmed reduction (TPR) experiments were conducted on a chemisorption station (Autosorb-1, Quantachrome Instruments). Approximately 100 mg catalyst was added in a quartz tube and heated to 700 °C at the rate of 10 °C/min under a 50 ml/min flow of 2% H_2 in Ar. The outlet H_2 and generated H_2S were monitored by a mass spectrometer (RGA 200 Stanford Research Systems, Inc.).

2.2. Catalyst evaluation

Hydrotreatment of canola oil over unsupported catalyst CoMoS or NiMoS was performed in a batch reactor (Parker Autoclave Engineers Inc.) under pressure of 9 MPa hydrogen (99.99%) at 375 °C. The catalyst to feed ratio was set at 1:200 by weight. Reaction was kept for 8 h, and liquid products were sampled during the reaction. Hydrogen was supplemented once the pressure dropped below 8.6 MPa. The external mass transfer was assumed negligible because of the high agitation of 1000 rpm, while internal mass transfer was ignored, since catalyst was nano-sized fines.

2.3. Product analysis

The fatty acids in triglycerides of canola oil were analyzed following the procedure described elsewhere [6]. Triglycerides were first converted to their corresponding fatty acid methyl esters and then analyzed by a gas chromatography–mass spectrometry (Shimadzu GCMS-QP5000) with a weak-polarity column (Agilent J&W HP-5).

The liquid compounds were identified with a GC–MS (Shimadzu GCMS-QP5000). The hydrocarbons were quantified using a Varian 450 gas chromatography with a hydrogen flame ionization detector and a non-polarity capillary column (Agilent J&W VF-1ms). The boiling point distribution of the final liquid products was estimated using a Shimadzu GC-2010 following ASTM-2887.

The canola oil and upgraded products were examined on a CHNS-O 932 elemental analyzer (LECO Corporation, MI, US) following ASTM D5291-10. Oxygen content was obtained from the balance. Total acidity number (TAN) was measured using an automatic potentiometric titrator following ASTM D664. The concentration of alcohols and aldehydes was tested using Shimadzu GCMS-QP5000. The content of unreacted glycerides was calculated from the balance.

Table 1
Basic properties of NiMoS and CoMoS.

Catalysts	NiMoS	CoMoS
Promoter/(promoter + Mo)	0.24	0.25
Average slab length (nm)	10.36	7.80
Average layer numbers	4.75	2.92
Fraction of edge metal atoms	0.116	0.151
BET surface area (m^2/g)	37.8	82.2
Total pore volume (cm^3/g)	0.257	0.526
Fraction of S loss (%)[a]	6.8	3.3

[a] Fraction of S loss is calculated from the difference of sulfur content between fresh and spent catalyst.

The liquid samples were analyzed using a Fourier transform infrared spectrometer (Nicolet 6700 FTIR, Thermo Scientific, US) in the range of 400–4000 cm^{-1} at a resolution of 4 cm^{-1}. Density of the liquid oils was tested using a portable density meter (DMA 35N, Anton Paar GmbH, Graz, Austria) following ASTM-7777.

CO and CO_2 were analyzed using a mass spectrometer (RGA 200). Gaseous hydrocarbons (C_1—C_6) were determined on a Shimadzu GC-17A equipped with a flame ionization detector (FID).

2.4. Calculations

The catalyst activity is expressed in terms of glycerides conversion and oxygen removal rate, as shown in Eqs. (1) and (2), respectively.

$$\text{glycerides conversion} = 1 - \frac{\text{glycerides in liquid product}}{\text{glycerides in canola oil}} \quad (1)$$

$$\text{oxygen removal rate} = 1 - \frac{\text{oxygen in liquid product}}{\text{oxygen in canola oil}} \quad (2)$$

Comparison of different oxygen elimination reactions (HDO and HDC) is presented by the ratio of generated C_{18} to C_{17} hydrocarbons in the following equation

$$C_{18}/C_{17}\ \text{ratio} = \frac{\text{mass of } C_{18} \text{ hydrocarbons}}{\text{mass of } C_{17} \text{ hydrocarbons}} \quad (3)$$

The hydrocracking and polymerization degree is calculated by Eqs. (4) and (5), respectively.

$$\text{hydrocracking degree} = \frac{\text{mass of } \sum C_i (i < 15)}{\text{mass of total hydrocarbons}} \quad (4)$$

$$\text{polymerization degree} = \frac{\text{mass of } \sum C_i (i > 18)}{\text{mass of total hydrocarbons}} \quad (5)$$

Hydrogenation activity is reflected by paraffin selectivity in the following equation

$$\text{paraffin selectivity} = \frac{\text{mass of paraffins}}{\text{mass of total hydrocarbons}} \quad (6)$$

3. Results

3.1. Unsupported catalyst

The crystalline structures of nanosized unsupported CoMoS and NiMoS catalysts are identified by TEM images (Fig. 1). CoMoS crystalline shows well dispersed small particles (Fig. 1a) and short slabs (Fig. 1c), while NiMoS appears to be more agglomerative (Fig. 1b) and longer in length (Fig. 1d). The main properties of the catalysts are listed in Table 1. The average layer number and slab length for CoMoS are 2.92 and 7.8 nm, respectively, while, for NiMoS, are 4.75 and 10.36 nm. Using the method described by Calais et al. [15], the fraction of edge metal atoms on catalysts are calculated,

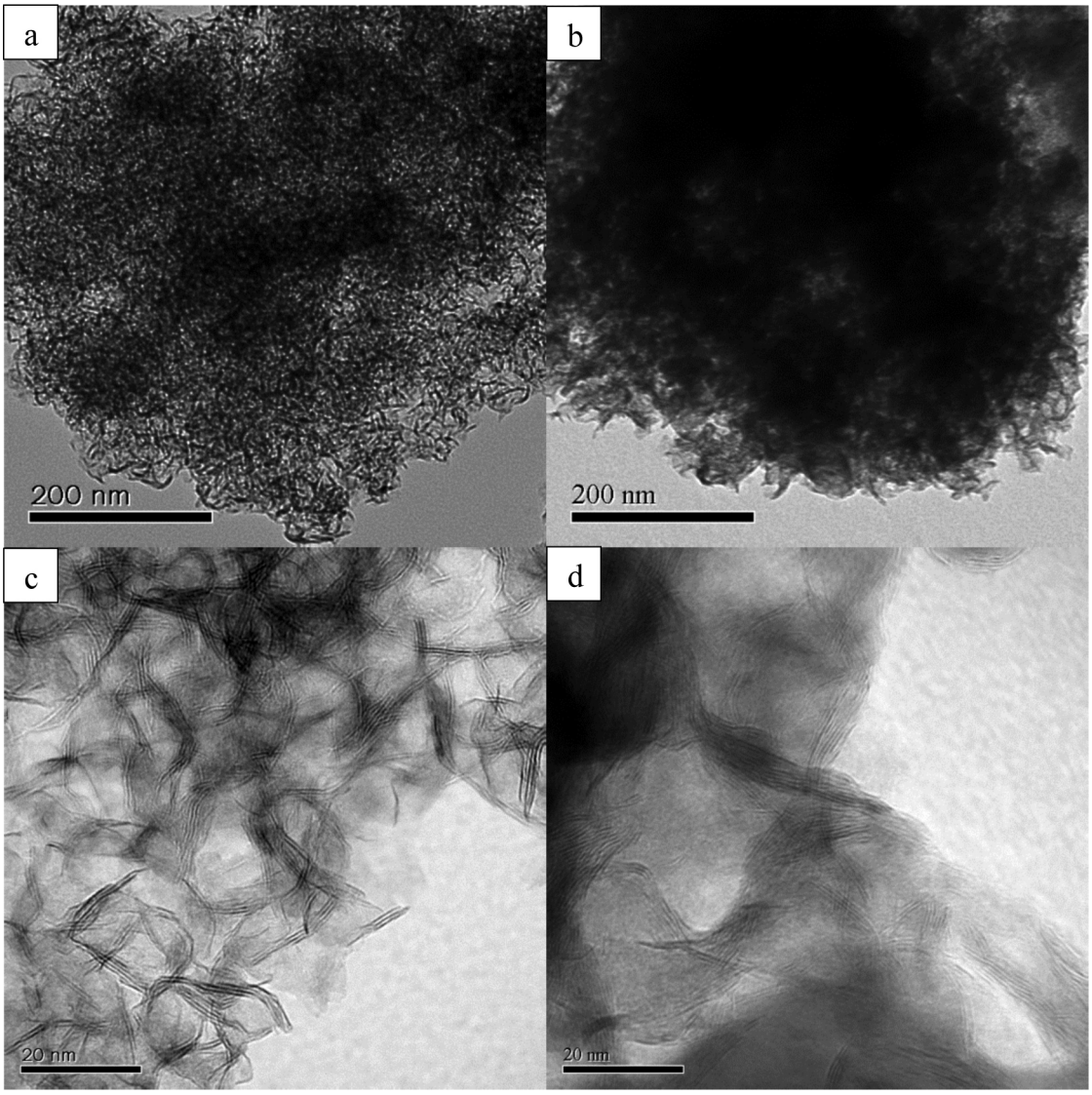

Fig. 1. TEM images of unsupported catalysts (a) and (c) CoMoS; (b) and (d) NiMoS.

which shows that Co-promoted catalyst has more edge sites than Ni-promoted catalyst does. EDX results show the atomic ratios of Co and Ni to total metals are 25% and 24%, respectively. The S contents of spent CoMoS and NiMoS drop 3.3% and 6.8%, respectively, in comparison with the corresponding fresh catalysts. The loss of sulfur is probably due to oxygen replacement on the edge of sulfur sites.

The surface area and pore volume of nickel and cobalt promoted catalysts are also shown in Table 1. CoMoS has larger surface area and pore volume than NiMoS does. In Fig. 2, a bimodal pore size distribution is observed for CoMoS with a sharp peak at 2.5 nm and a broad peak at around 12 nm. Similar pore size distribution is also found for NiMoS but with lower peak height.

The TPR spectra shown in Fig. 3 are quantitatively summarized in Table 2. As expected, the total consumption of H_2 by CoMoS is higher, which is consistent with more calculated edge sites of CoMoS (Table 1). However, H_2S is not generated over CoMoS until temperature is higher than 400 °C. NiMoS behaves differently. H_2S is detected simultaneously with the consumption of H_2 and the amount of produced H_2S is similar to the consumption of H_2.

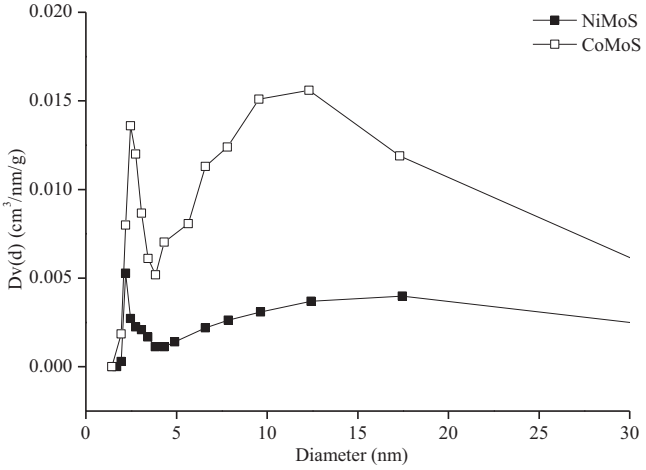

Fig. 2. BJH pore size distribution of unsupported catalysts.

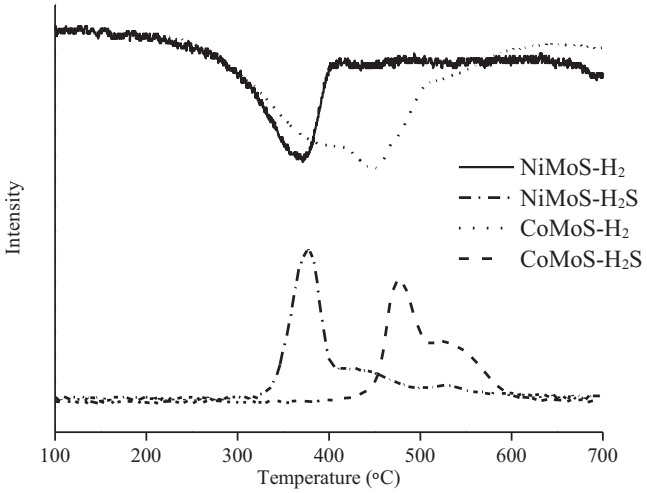

Fig. 3. TPR spectra of unsupported catalysts CoMoS and NiMoS.

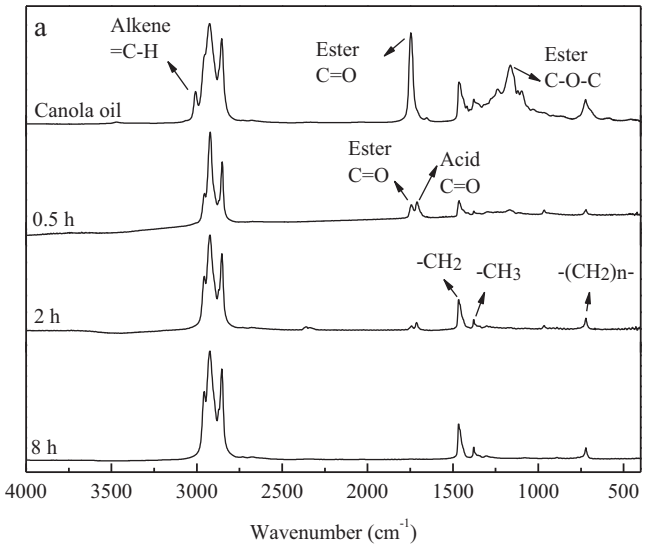

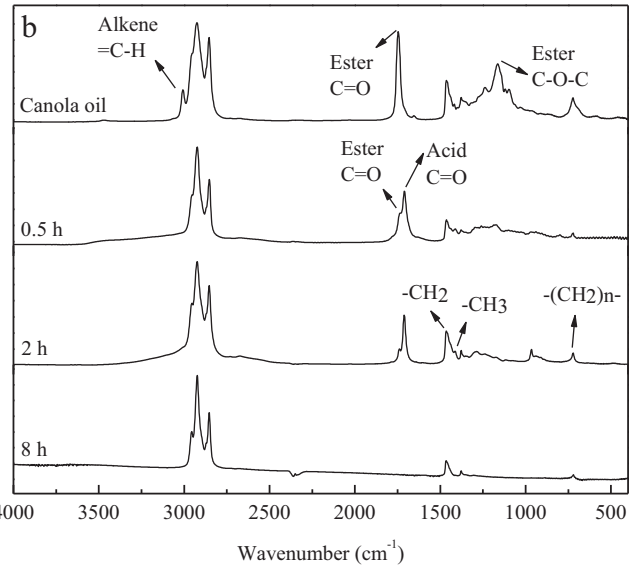

Fig. 4. FTIR spectra of hydrotreated canola oil. Catalysts: (a) NiMoS; (b) CoMoS. Ester C=O: 1742 cm^{-1}; Ester C—O—C: 1170 cm^{-1}; Fatty acid C=O: 1711 cm^{-1} C=C: >3000 cm^{-1}; C—H: 3000–2800 cm^{-1}; CH_2 and CH_3: 1475–1300 cm^{-1}; —$(CH_2)_n$—:722 cm^{-1}.

3.2. Deoxygenation activity

Triglycerides are the main components of canola oil with a small amount of free carboxylic acids at a total acidity number (TAN) of 2.89 (Table 3). The distribution of fatty acids is listed in Table 4, which shows that there are only acids with even-numbered carbon atoms. C_{18} fatty acids are dominant component of canola oil, most of which are unsaturated carbon chains. After 8 h hydrotreatment, the oxygen was completely removed over both catalysts. The TAN of hydrotreated liquid products are close to 0, indicating a complete conversion of carboxylic acids (Table 3).

Under the hydrotreating condition, triglycerides are first converted to the corresponding fatty acids which will be further transformed to hydrocarbons through two main reaction pathways: hydrodeoxygenation and hydrodecarbonylation/decarboxylation. The development of deoxygenated products was observed by FTIR (Fig. 4). For NiMoS, the two peaks characterizing the absorption of ester C=O and C—O—C are significantly smaller than that of feedstock at the first 0.5 h of reaction, indicating a quick decomposition of triglycerides. After 2 h, most of esters and fatty acids are transformed as the intensity of the peaks is significantly dropped. The complete conversion of triglycerides/fatty acids is reached at 8 h because only the absorption for alkanes is observed (Fig. 4a). On the other hand, a slow decomposition rate of triglycerides/fatty acids over CoMoS is noted. Strong adsorption spectra characterizing fatty esters and acids are observed at 0.5 h of reaction (Fig. 4b). Figs. 5 and 6 compare the glyceride conversion and oxygen removal rates over catalysts CoMoS and NiMoS. Within the first 3 h of reaction, NiMoS exhibits higher glycerides conversion and oxygen removal rate than CoMoS. The maximum differences in glycerides conversion and oxygen removal rate are 8% and 34%, respectively.

3.3. Product selectivity

3.3.1. C_{18}/C_{17} ratio

The mass balance for both catalysts is carried out after 8 h' reaction (Table 5). The sums of gas and liquid products over CoMoS and NiMoS reach 96.2% and 96.7%, respectively. The C_{18}/C_{17} ratios are compared in Fig. 7. It is noticed that the C_{18}/C_{17} ratio obtained with NiMoS (1.7) is much higher than that over CoMoS (0.5) in the entire

Table 2
TPR data summary.

Catalysts	H_2 consumption		Corresponding H_2S production	
	Peak temperature (°C)	Amount ($\times10^{-3}$ mol/g cata)	Peak temperature (°C)	Amount ($\times10^{-3}$ mol/g cata)
NiMoS	230–415	2.34	310–415	2.25
CoMoS[a]	230–430	2.56	402–510	1.26

[a] Calculation based on the first peak.

Table 3
Properties of the feed and hydrotreated products (8 h).

Oils	Density (g/ml) at 25 °C	TAN number (mg KOH/g)	Oxygen content (%)
Canola oil	0.9179	2.89	11.66
HCO1[a]	0.7801	0	0
HCO2[b]	0.8004	0.01	0

[a] Hydrotreated canola oil over catalyst NiMoS.
[b] Hydrotreated canola oil over catalyst CoMoS.

Table 4
Fatty acid composition of canola oil tested by GC–MS.

Fatty acids (Cn:m)[a]	C16:0	C16:1	C18:0	C18:1	C18:2	≥C20:0
Content (wt.%)	5.9	0.4	1.3	73.4	17.7	0.6

[a] Cn:m: n, number of carbon atoms; m, number of C=C double bonds in fatty acids.
e.g. C16:1, fatty acid with 16 carbon atoms and 1 C=C double bond.

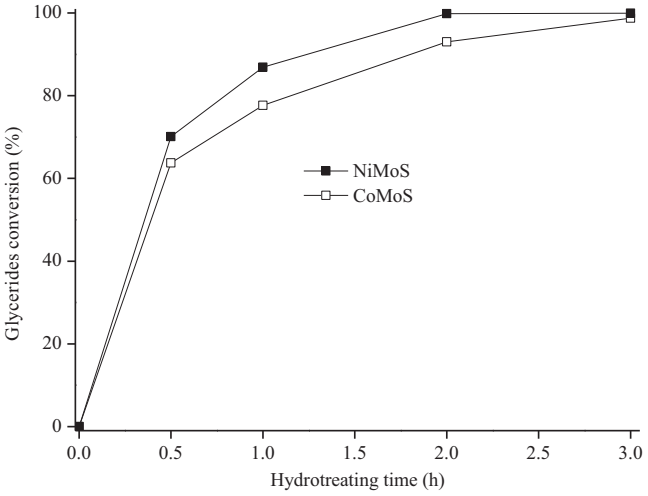

Fig. 5. Comparison of glycerides conversion.

course of the reaction. High C_{18}/C_{17} ratio over NiMoS suggests that HDO is the main pathway. Oxygen is removed in the form of H_2O in HDO route. On the other hand, HDC is favorable on CoMoS, with the formation of CO or CO_2 (Table 5). In addition, hydrodecarbonylation is more favored than decarboxylation on CoMoS, evidenced by the formation of more CO than CO_2. There is no obvious evidence

Table 5
Hydrotreated product distribution.

Products (wt.%)	Hydrotreated over NiMoS	Hydrotreated over CoMoS
Liquid	90.3	86.0
CO	3.4	6.1
CO_2	1.3	1.6
Methane C_1	0.1	0.2
C_2—C_6	1.6	2.3
Mass balance	96.7	96.2

Hydrogen was not considered in the mass balance calculation.

of the formation of methane from the reduction of carbon oxide, as seen from the low methane content (Table 5).

3.3.2. Hydrocracking and polymerization degree

Canola oil is composed of 99 wt.% C_{16} and C_{18} fatty acids. C_{15} to C_{18} hydrocarbons are the corresponding hydrotreated products [4]. Therefore, hydrocarbons with carbon number lower than 15 and higher than 18 are the hydrocracking and the polymerization products. After 8 h hydrotreatment, approximately 14% of the canola oil is hydrocracked and polymerized on CoMoS. In contrast, less than 7% of feed is observed with NiMoS (Fig. 8). This indicates higher degree of hydrocracking and polymerization occurs over CoMoS. Simulated distillation results show a dramatic decrease of heavy components after hydrotreatment on both catalysts. NiMoS shows good performance with high selectivity to diesel-like hydrocarbons In contrast, high yields of gasoline-like hydrocarbons and heavy components are obtained over CoMoS

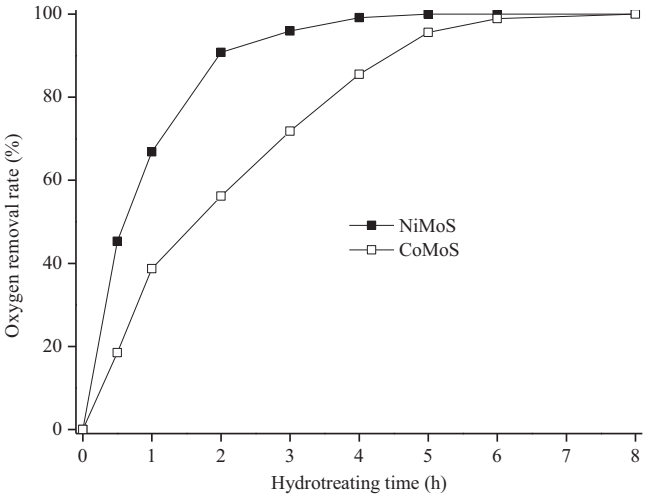

Fig. 6. Comparison of deoxygenation activities.

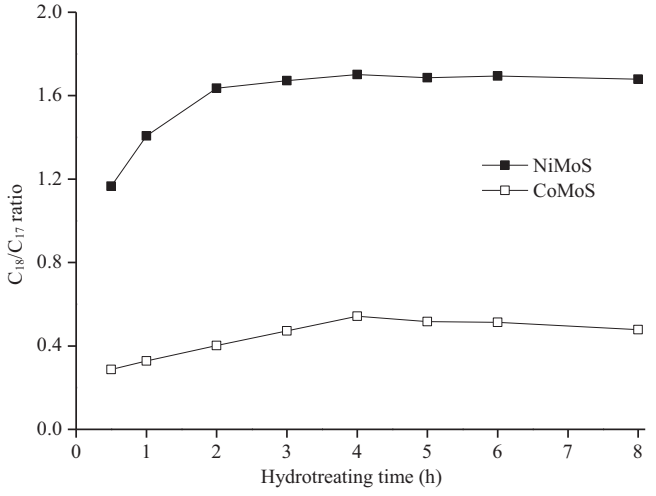

Fig. 7. Comparison of C_{18}/C_{17} ratio.

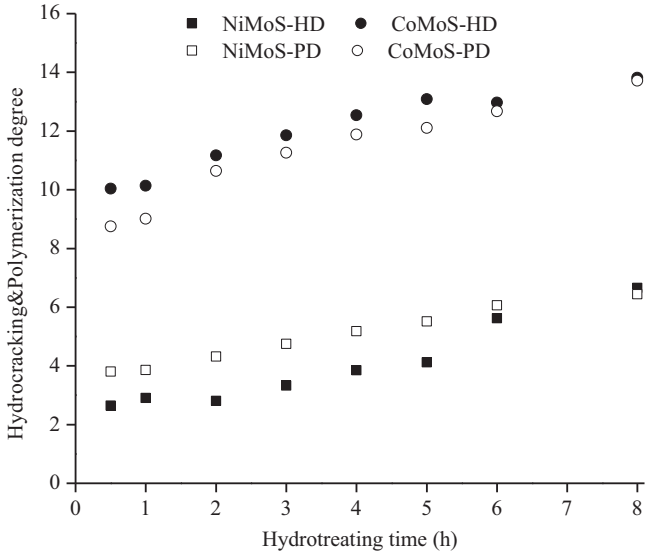

Fig. 8. Comparison of hydrocracking and polymerization degree. HD: hydrocracking degree; PD: polymerization degree.

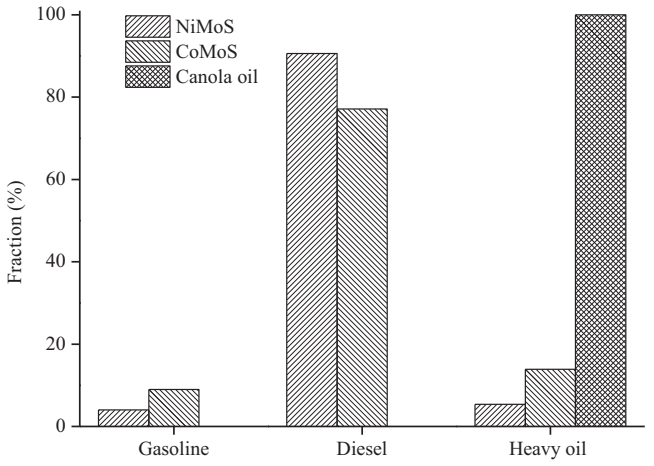

Fig. 9. Distribution of hydrocarbon products from simulated distillation. Gasoline: boiling point (BP) < 200 °C; Diesel: BP 200–350 °C; Heavy oil: BP > 350 °C.

(Fig. 9). It is indicated that cobalt promotes the breakage and formation of C—C bonds.

3.3.3. *Paraffin selectivity*

Fig. 10 shows that, at the end of the reaction, over 90% hydrocarbons are saturated over NiMoS, while nearly 40% hydrocarbons still contain double bonds when using CoMoS. This suggests that NiMoS has higher hydrogenation activity than CoMoS. The observation is also supported by the H/C molar ratio (Fig. 11). The H/C ratios increase with the conversion of oxygenates. Much higher H/C ratios are observed over NiMoS than over CoMoS. It confirms high hydrogenation activity of NiMoS.

4. Discussion

Deoxygenation of plant oils (triglycerides) using conventional supported sulfide catalysts has been well studied [9,16]. Disagreements in the main reaction pathways remain unsolved. Catalyst support materials play a key role in reaction pathways [12,13]. In this work, unsupported sulfided catalysts were used so that the interference by catalyst support was eliminated. It has been observed that Ni-doped MoS_2 catalyst promotes

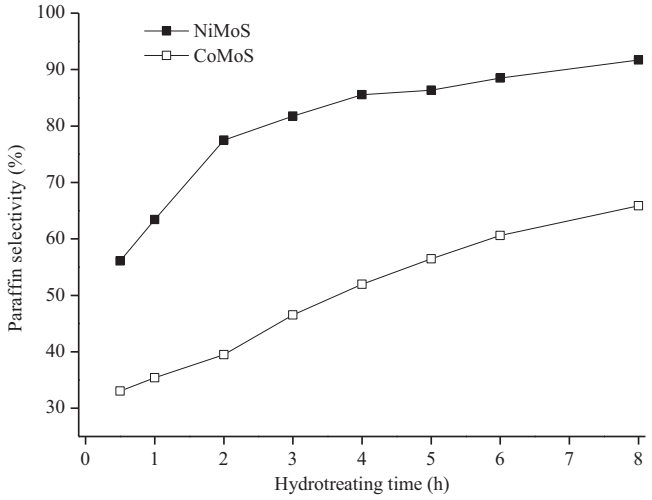

Fig. 10. Comparison of paraffin selectivity.

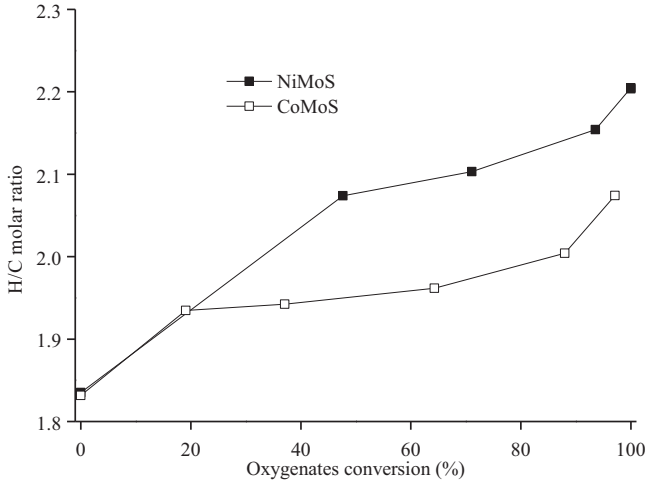

Fig. 11. Comparison of H/C molar ratio.

hydrodeoxygenation reaction, ending up with C_{18} hydrocarbons as a main liquid product. Co-promoted MoS_2 catalyst favors hydrodecarbonylation/decarboxylation reaction, resulting in more C_{17} hydrocarbons produced (Fig. 7). The distinct roles of Ni and Co are attributed to the difference of their structures. Ni-promoted catalyst contains abundant sulfur vacancies, whereas CoMoS has none until 400 °C, evidenced by the TPR results shown in Fig. 3. Consequently, at the reaction temperature of 375 °C, the main active sites of Ni-promoted catalyst are the unsaturated sites; on the contrary, saturated sites dominate the catalyst promoted by Co. The observation well agrees with the density function theory (DFT) calculation that nickel favors to be on the Mo-edge of MoS_2 and cobalt tends to substitute the Mo on the S-edge [17–19]. Therefore, the reactions over Ni-promoted catalyst tend to occur on the unsaturated metal edge, while the reactions over Co-promoted catalyst are likely to take place on saturated sulfur edge. The distinct active sites of the catalysts may be responsible for different main reaction pathways. It is worth noting that unsaturated sites would be created on CoMoS in a long-time hydrotreating reaction, and saturated sites are also present on NiMoS, especially at the beginning of the reaction. The following discussion only focuses on the main reaction pathways on both catalysts.

The main reaction mechanism over NiMoS at unsaturated metal edge is proposed in Scheme 1 (S1 hereafter). Firstly, hydrogen is dissociated and adsorbed on unsaturated Mo atom and S atom,

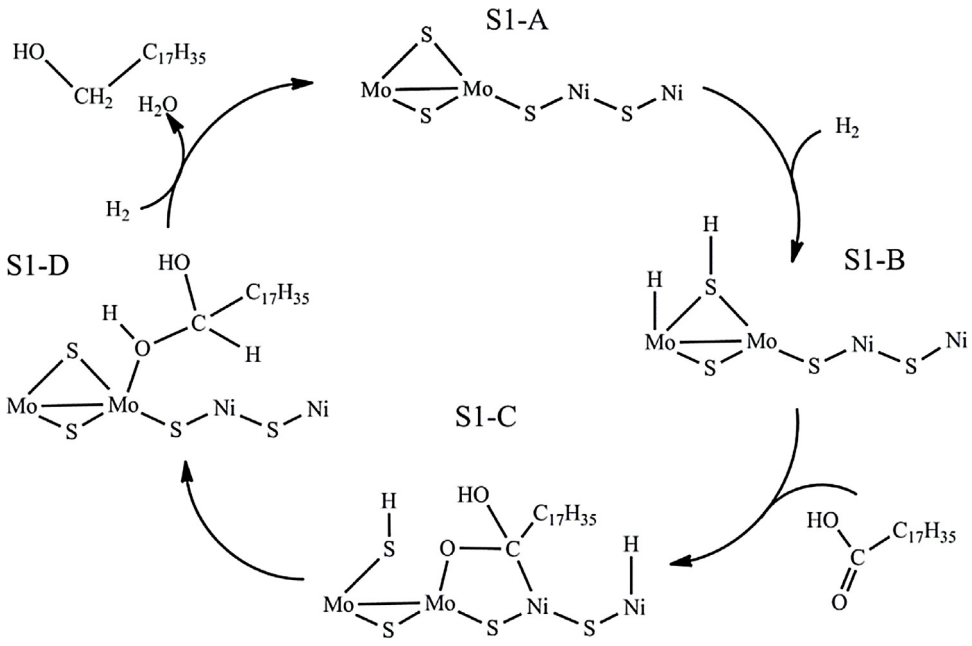

Scheme 1. Main deoxygenation mechanism on NiMoS.

forming S—H and Mo—H at the S vacancies (S1-B). Formation of the Mo—H and S—H pair is exothermal and requires the minimal dissociation energy [20]. The high electrophilic Mo atom tends to adsorb O atom in C=O bond as O tends to be more nucleophilic in C=O than in C—O—C. Introduction of Ni promotes disruption of π bond on O=C to form a —Mo—O—C—Ni— cycle (S1-C). This "synergy effect" displayed by NiMoS has been recently explained by the DFT theory. The presence of Ni can reduce the energy barriers for O=C bond [21]. S1-C is a critical step for Ni to realize its promoting effect on MoS_2 catalysts. S vacancies are essential in providing the sites for Mo and Ni to bond O and C atoms. With dissociative adsorbed H in the vicinity, Ni—C scission proceeds readily. Dissociated H preferentially interacts with C and O to form C—H and O—H bonds (S1-D) [21,22]. Surrounded by abundant dissociated H on Mo and S atoms, the C—O splitting is likely to take place with alcohol and water as products. Alcohol will undergo another C—O

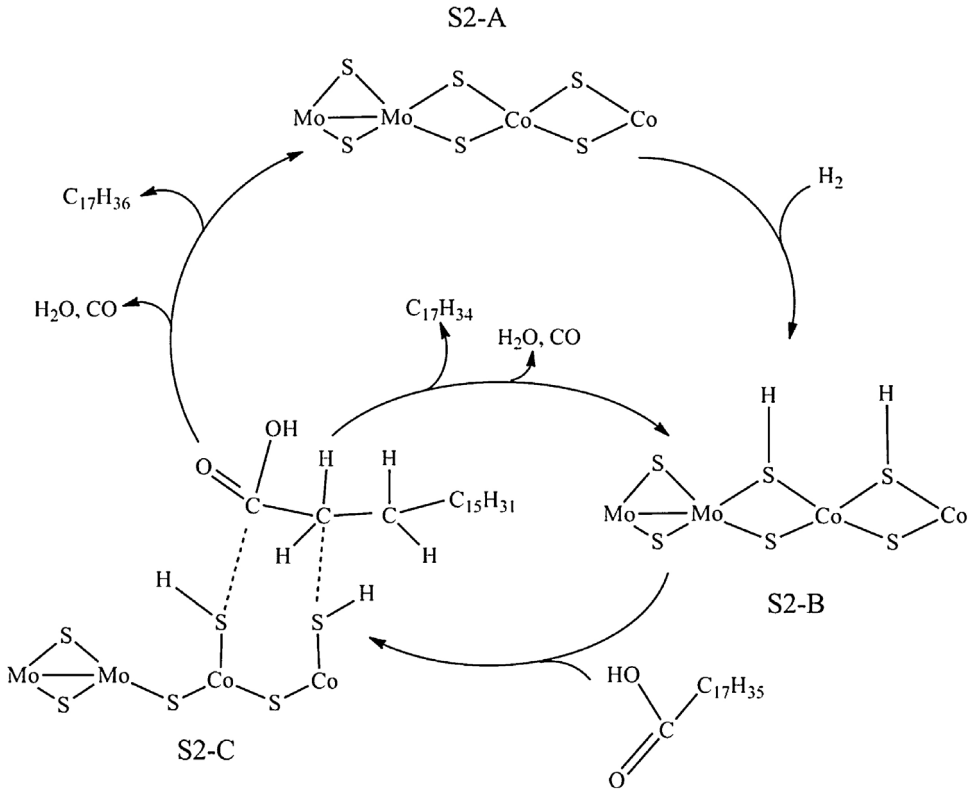

Scheme 2. Main deoxygenation mechanism on CoMoS.

scission to form *n*-octadecane or *n*-octadecene. The generation of alcohol is essential for C_{18} production and determines the main deoxygenation.

The main reaction mechanism over Co-promoted MoS_2 is demonstrated in Scheme 2 (referred as S2). High H_2 consumption over CoMoS in the TPR test indicates that cobalt can facilitate hydrogen adsorption on sulfur sites generating stable H—S bonds (S2-B). This phenomenon is consistent with the published DFT calculations that (Co-) SH group is the most stable hydrogen species on the Co-promoted S-edge [23,24]. The weaker bonding between S and Co atoms opens the door to strong interaction between the terminal S and H atoms [23,24]. The formed HS groups are highly nucleophilic and attractive to the electrophilic C atoms with or adjacent to a carboxyl group (S2-C). And then the scission of weakened C—C bond is followed by forming *n*-heptadecane or *n*-heptadecene and by-product formic acid, which can be easily decomposed to CO and H_2O [25–27]. It is noted that saturated sulfur sites providing C atom adsorption sites essentially contribute to the HDC reaction route.

Scheme 1 suggests a deoxygenation mechanism for C=O over NiMoS. The compounds containing C=O bonds, such as acids, aldehydes, etc. most likely undergo the same pathways over NiMoS in elimination of oxygen. The finding is highly agreed with the result of model compounds, e.g. ethyl heptanoate, heptanoic acid, etc. [22]. The compounds that do not have C=O bonds but an aromatic structure (e.g. phenol), the synergy effect (shown in Scheme 1) may not be able to established. Scission of C—-O may be achieved through hydrogenation. Yoosuk et al. observed that more hydrogenated products such as cyclohexane were produced than benzene when phenol was treated over a NiMoS catalyst [28]. With the same reactant, more benzene produced over CoMoS, which indicated direct C—O splitting was more favorable than C—O cleavage through hydrogenation [29]. For petroleum components, such as dibenzothiophene (DBT), similar trend was observed that selectivity in hydrogenation (HYD) pathway on NiMoS was higher than on CoMoS [30,31].

The high hydrogenation ability of NiMoS was also observed in this work, where a high degree of saturation was observed (Fig. 10). CoMoS exhibits higher hydrocracking activity (Figs. 8 and 9). The TPR results obtained in this work lead to a conclusion that hydrocracking activity is facilitated by saturated active sites on sulfur edge, while hydrogenation favors to take place at sulfur vacancies located at the edges of active metal sites. The findings are in good agreement with the literatures, where it was reported that SH groups promoted hydrogenolysis and hydrogenation took place on the unsaturated metal sites [32,33].

In a common practice, MoS_2 is loaded on porous materials, such as Al_2O_3. Comparing our results to the supported catalysts reported in the literatures may lead a way to understand the role of support in deoxygenation. The hydrocarbons generated over most supported Co(Ni)MoS catalysts show higher C_{18}/C_{17} ratios than the ratio obtained over their unsupported counterparts [7,9]. There is no distinct performance difference observed between supported CoMoS and NiMoS [8]. It is generally accepted that the Lewis acid sites on Al_2O_3 supports increases the activity of hydrogenation and dehydration reactions, which indicates catalyst support, e.g. Al_2O_3, enhances the HDO pathway [13]. It suggests that catalyst support plays a role in deoxygenation and the presence of catalyst support covers the different behaviors of active phases-NiMoS and CoMoS.

5. Conclusions

Unsupported Ni and Co-promoted MoS_2 catalysts were studied in deoxygenation of raw canola oil. The TEM images show CoMoS has more edge sites; the TPR results indicate that Co-promoted catalyst has high ability to adsorb H_2. Sulfur vacancies can be barely observed until 400 °C. Compared to CoMoS, NiMoS exhibits lower amount of edge sites but higher ability to create sulfur vacancy at low temperature. Different properties lead to their distinct performances in hydrotreatment of canola oil in term of activity and selectivity. NiMoS presents a higher deoxygenation activity than CoMoS. NiMoS exhibits high selectivity toward C_{18} (HDO product) with a C_{18}/C_{17} ratio of 1.7, generates low hydrocracking and polymerization side reactions and produces more paraffins over olefins when plant oil is used as feed.

Promoter Ni is primarily functioned through the synergy effect of Mo and Ni on unsaturated metal sites while Co facilitates HDC reaction routes by activating the saturated sulfur sites. The higher hydrocracking (C—C hydrogenolysis) activity of CoMoS indicates hydrocracking tends to occur on the saturated sites; the high hydrogenation capacity of NiMoS implies sulfur vacancies are likely to be involved in hydrogenation.

Acknowledgments

The authors gratefully acknowledge the financial assistance from Canada Research Chairs program, Natural Sciences and Engineering Research Council of Canada and Canada Foundation for Innovation.

References

[1] E. Laurent, B. Delmon, Ind. Eng. Chem. Res. 32 (1993) 2516–2524.
[2] V.N. Bui, D. Laurenti, P. Afanasiev, C. Geantet, Appl. Catal., B: Environ. 101 (2011) 239–245.
[3] D. Kubicka, L. Kaluza, Appl. Catal., A: Gen. 372 (2010) 199–208.
[4] G.W. Huber, P. O'Connor, A. Corma, Appl. Catal., A: Gen. 329 (2007) 120–129.
[5] O.I. Senol, E.M. Ryymin, T.R. Viljava, A.O.I. Krause, J. Mol. Catal. A: Chem. 268 (2007) 1–8.
[6] P. Simacek, D. Kubicka, G. Sebor, M. Pospisil, Fuel 88 (2009) 456–460.
[7] P. Simacek, D. Kubicka, G. Sebor, M. Pospisil, Fuel 89 (2010) 611–615.
[8] M. Toba, Y. Abe, H. Kuramochi, M. Osako, T. Mochizuki, Y. Yoshimura, Catal. Today 164 (2011) 533–537.
[9] M. Krar, S. Kovacs, D. Kallo, J. Hancsok, Bioresour. Technol. 101 (2010) 9287–9293.
[10] S. Bezergianni, A. Dimitriadis, T. Sfetsas, A. Kalogianni, Bioresour. Technol. 101 (2010) 7658–7660.
[11] D. Kubicka, M. Bejblova, J. Vlk, Top. Catal. 53 (2010) 168–178.
[12] A. Centeno, E. Laurent, B. Delmon, J. Catal. 154 (1995) 288–298.
[13] E.M. Ryymin, M.L. Honkela, T.R. Viljava, A.O.I. Krause, Appl. Catal., A: Gen. 389 (2010) 114–121.
[14] H. Zhang, H. Lin, W. Wang, Y. Zheng, P. Hu, Appl. Catal., B: Environ. 150–151 (2014) 238–248.
[15] C. Calais, N. Matsubayashi, C. Geantet, Y. Yoshimura, H. Shimada, A. Nishijima, M. Lacroix, M. Breysse, J. Catal. 174 (1998) 130–141.
[16] T.M. Sankaranarayanan, M. Banu, A. Pandurangan, S. Sivasanker, Bioresour. Technol. 102 (2011) 10717–10723.
[17] J.F. Paul, E. Payen, J. Phys. Chem. B 107 (2003) 4057–4064.
[18] M. Brorson, A. Carlsson, H. Topsoe, Catal. Today 123 (2007) 31–36.
[19] P.G. Moses, B. Hinnemann, H. Topsoe, J.K. Norskov, J. Catal. 248 (2007) 188–203.
[20] I. Borges Jr., A.M. Silva, A.P. Aguiar, L.E.P. Borges, J.C.A. Santos, M.H.C. Dias, J. Mol. Struct. THEOCHEM 822 (2007) 80–88.
[21] C. Dupont, R. Lemeur, A. Daudin, P. Raybaud, J. Catal. 279 (2011) 276–286.
[22] M.R. de Brimont, C. Dupont, A. Daudin, C. Geantet, P. Raybaud, J. Catal. 286 (2012) 153–164.
[23] A. Travert, H. Nakamura, R.A. van Santen, S. Cristol, J.-F. Paul, E. Payen, J. Am. Chem. Soc. 124 (2002) 7084–7095.
[24] M.Y. Sun, A.E. Nelson, J. Adjaye, J. Catal. 233 (2005) 411–421.
[25] S. Brunet, D. Mey, G. Perot, C. Bouchy, F. Diehl, Appl. Catal., A: Gen. 278 (2005) 143–172.
[26] O.I. Senol, T.R. Viljava, A.O.I. Krause, Appl. Catal., A: Gen. 326 (2007) 236–244.
[27] S. Czernik, A.V. Bridgwater, Energy Fuels 18 (2004) 590–598.
[28] B. Yoosuk, D. Tumnantong, P. Prasassarakich, Fuel 91 (2012) 246–252.
[29] B. Yoosuk, D. Tumnantong, P. Prasassarakich, Chem. Eng. Sci. 79 (2012) 1–7.
[30] B. Yoosuk, J.H. Kim, C. Song, C. Ngamcharussrivichai, P. Prasassarakich, Catal. Today 130 (2008) 14–23.
[31] J.H. Kim, X.L. Ma, C.S. Song, Y.K. Lee, S.T. Oyama, Energy Fuels 19 (2005) 353–364.
[32] B. Delmon, Catal. Lett. 22 (1993) 1–32.
[33] A.Y. Bunch, U.S. Ozkan, J. Catal. 206 (2002) 177–187.